Vessel-contrast enhancement in label-free optical coherence angiography based on phase and amplitude speckle variability

Lev A. Matveev[1,2*], Valentin Demidov[3], Alexander A. Moiseev[1], Grigory V. Gelikonov[1,2], Alexandr L. Matveyev[1,2], Valentin M. Gelikonov[1,2], Maria M. Karabut[2], Ekaterina V. Gubarkova[2], Elena S. Finagina[2], Marina A. Sirotkina[2], Anna V. Maslennikova[2], Natalia D. Gladkova[2], Alex Vitkin[2,3], Vladimir Yu. Zaitsev[1,2]

[1]Institute of Applied Physics Russian Academy of Sciences, Ulyanova Street 46, 603950 Nizhniy Novgorod, Russia
[2]Nizhny Novgorod State Medical Academy, Minin Square 10/1, 603005 Nizhny Novgorod, Russia
[3]University of Toronto and University Health Network, 610 University Ave., Toronto, Ontario, M5G 2M9, Canada

ABSTRACT

Recently proposed *in vivo* label-free optical coherence angiography techniques based on phase and amplitude speckle variability often require additional signal pre- and post processing operations to enhance vessel-contrast. Here, we discuss 1) contrast enhancement by optimizing the signal normalization/weighing before processing; 2) Kasai phase estimator based algorithm for phase compensation between processed A-scans to reduce masking role of motion artifacts; and 3) features of image projection through the imaging depth for *en face* plotting. We demonstrate the efficiency of these algorithms for in-vivo optical coherence angiography of hamsters' cheeks as a part of pre-clinical investigations, as well as preliminary microcirculation imaging of patients treated with radiation therapy. This technical framework complements our recent publications on M-Mode like OCT algorithm and its implementation.

Keywords: optical coherence tomography, angiography, image processing, speckle variance, flow diagnostics

1. INTRODUCTION

Label-free optical coherence angiography utilizes temporal variability of speckle structure in subsequently optical coherence tomography (OCT) two-dimensional cross-sections (frames) of imaged tissues[1,2,3]. Both phase and amplitude of complex-valued OCT signals can be processed to isolate vessels and estimate their parameters[1,2,4,5,6]. However, in real in-vivo imaging straightforward processing often fails due to a number of interfering factors. First of all, these factors comprise endogenous and exogenous tissue motions[4], surface-structure artifacts[5], and tissue signal-to-noise ratio (SNR) inhomogeneity[2,7,8]. Here, we describe procedures intended to reduce negative effects of the above-mentioned factors that were not discussed in our recent publications[4,5,6]:

1. To avoid the outbalancing contribution of uneven pixels' amplitudes to speckle variability we normalize the complex-valued signal to the square root of its amplitude for each pixel;

2. To reduce the tissue motion artifacts we perform for each temporal sequence of processed A-scans cumulative mean phase equalization procedure based on Kasai estimator;

3. To reduce the contribution of "noise" pixels to resulting microcirculation maps we apply binary Heaviside mask and choose an appropriate type of *en-face* projection (maximum intensity projection or or average intensity projection).

For the experimental demonstrations, we used a home-made spectral-domain OCT scanner described in our previous publications[7-13]. Briefly, it had a central optical wavelength of 1320 nm, bandwidth of 106 nm and a scan rate of 20 kHz for spectral fringes. The axial resolution of the system is 10 μm and in lateral full width half-maximum (FWHM) beam diameter is 20 μm. OCT system has 512 elements of spectrometer array in the axial direction.

*lionnn52rus@mail.ru; phone 7 831 436-7293; fax 7 831 436-5976; iapras.ru

Saratov Fall Meeting 2015: Third Annual Symposium Optics and Biophotonics; Seventh Finnish-Russian Photonics and Laser Symposium (PALS), edited by E. A. Genina, V. L. Derbov, D. E. Postnov, A. B. Pravdin, K. V. Larin, I. V. Meglinski, V. V. Tuchin, Proc. of SPIE Vol. 9917, 99171S · © 2016 SPIE · CCC code: 1605-7422/16/$18 · doi: 10.1117/12.2229740

During experiments with anesthetized rodents (hamster cheeks), we acquired 3D data sets covering 3x3 mm^2 areas. Scanning time is 7 minutes. The number of A-scans in each two-dimensional B-scan was 512 and the number of partially overlapped B-scans in each 3D data set was 16384. The scanning in slow direction (perpendicular to the B-scans) was continuous. Such an over-sampled acquisition allowed for accumulation of data, which was averaged during post-processing using a simple down sampling procedure of resulting angiogram. This feature enables better post-processing averaging for capturing variations of small capillaries with unstable (discontinuous) flow intensity.

In comparison with sleeping animals, clinical investigations on patients treated with radiation therapy require faster scan-pattern protocol to minimize the volumetric data acquisition time. In order to obtain the volumetric data set covering the same 3x3 mm^2 area in 52 seconds, we reduced the number of acquired A-scans to 256 for each B-scan and the number of acquired B-scans to 4096 while keeping continuous the scanning in slow direction (perpendicular to the B-scans). With this scanning pattern, A-scans did not overlap much, and the distance between A-scans in each B-scan was equal to 12 microns (in compare with FWHM beam diameter equals to 20 μm). The density of B-scans in 3D dataset was 8 times less in comparison with the animal scanning protocol. This means that the degree of accumulation/averaging were less accurate and the SNR for small vessels with discontinuous flow rate was lower but still sufficient for their detection.

It should be also noted that experiments with hamsters were performed in non-contact manner (i.e., the probe did not contact the tissue) while experiments with the patients in clinic (inner side of the mouth cheek) were performed in contact manner (tissue was stabilized by the glass window of the probe).

Acquired data was processed with high-pass filtering of complex-valued temporal variations of each pixel, which ensures that the resolution of resulting angiograms is the same as in structural OCT images (as described in ref.[4]). The filtering is applied to the slow scanning direction (inter-B-scan processing) and the threshold frequency is chosen to be 6 Hz. This is enough to filter out tissue slow motion signals and to isolate blood-particle motions against the "solid" tissue. Namely, slow motions (flows and Brownian motions) corresponding to speckle decorrelation times up to 160 ms become visualized.

Below we discuss the pre- and post-processing procedures that increase the vessel-contrast in the resulting images.

2. SIGNAL NORMALIZATION BEFORE PROCESSING

In order to reduce artifacts arising from the unbalanced points, we normalized the complex-valued signals of each pixel to square root of its time-averaged amplitude. By doing that, we normalize variations of pixel complex amplitudes, which increases the contribution of phase variations and reduce the role of abnormal pixels (i.e., those with saturation, glare, etc.)[5]. In our previous work we used even harder normalization by equalizing amplitudes of complex-valued signals and retaining only phase information[5]. Phase variation is initially limited and does not produce such amplitude-dependent (scale-dependent) spurious effects as those caused by amplitude variations of abnormal pixels. However, amplitude variations also contain valuable information in pixels corresponding to both the "solid" tissue and flows. Namely, speckles corresponding to fluctuating scatterers should vary in the order of its mean value (~100% variations) because speckle variations due to relative motions usually pass through constructive and destructive interference. Therefore, here we propose a softer normalization of each complex-valued pixel to the square root of its mean amplitude averaged over five temporal points. The efficiently of such a normalization procedure for vessel-contrast enhancement is demonstrated in Figure 1.

Figure 1 represents the en-face microvasculature maximum intensity projection (MIP) image processed by high-pass filtering of complex-valued signal. Figure 1(a) corresponds to the processing without preliminary normalization of the complex-valued pixels and Figure 1(b) with the above-described normalization. Figure 1(b) demonstrates how the above-described normalization helps to increases SNR of the vessels and enhance overall contrast of the vascular map. It should be noted here that in this image two other algorithms (phase compensation and binary mask multiplication) were also applied as described in the following sections.

It should also be noted that pre-processing vessel contrast enhancement in Figure 1(b) is not related to the scaling of the color axis, but is caused by improvement of vessels isolation and corresponding improvement of angiogram SNR due to the used amplitude normalization of the complex-valued signal in each pixel Indeed, there are two useful outcomes of this approach:

1) Firstly, it increases the weight of strong phase variations in fast decorrelating vessels. These vessels were blurred before and had decreased mean amplitude values caused by integration during the arrays exposure time.

2) Secondly, it discriminates saturated pixels that have weak phase variations and low relative amplitude variations (on order of a few per cent in comparison with the mean amplitude). Signals with very high mean amplitude and therefore, high absolute amplitude of these variations, after pre-processing normalization will not pass through the high-pass filter and will cause the artifacts. Normalization reduces the masking role of such abnormally strong amplitude variations with small relative values, because this means that normalization translates the variation from absolute to relative values. At the same time it is also perform better isolation of weakly scattering vessels with high relative amplitude and/or phase variation.

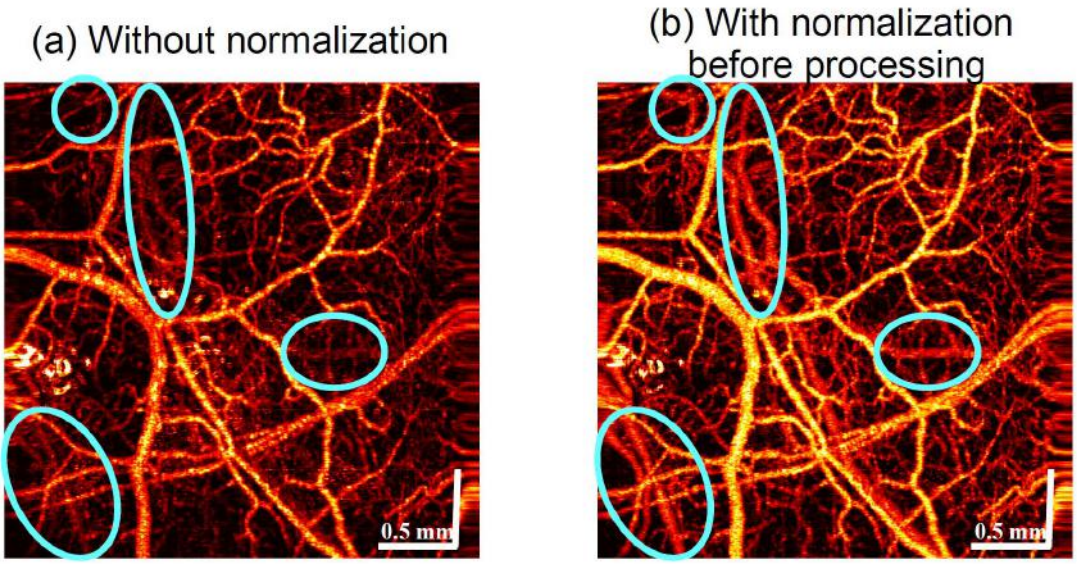

Fig.1. Demonstration of vascular contrast enhancement with pre-processing normalization algorithm. Panel (a) - *en face* microvasculature maximum-intensity projection (MIP) image processed by high-pass filtering of the complex-valued signal without pre-processing signal normalization; panel (b) - *en face* microvasculature MIP image obtained by the same filtering of the normalized signal. For both cases the same raw dataset was processed. The MIP's depth range is 600 microns, the imaging area is 3x3 mm^2, and the chosen threshold frequency of the high-pass filter is six Hz. As can be seen in the images, pre-processing signal normalization significantly increases SNR of the vessels and therefore enhance overall contrast of the vascular map. To highlight the most improved areas we marked these areas by ellipses. Contrast of many other not-marked vessels in the panel (b) in comparison with panel (a) is also significantly enhanced.

3. CUMULATIVE EQUALIZATION OF A-SCANS' MEAN PHASE BASED ON KASAI ESTIMATOR

The goal of this pre-processing procedure is to reduce the noisy contribution of tissue translational motions into resulting filtered microvasculature images. To suppress the masking influence of such motions, we perform A-scan phase equalization based on Kasai estimation[14] of mean phase difference of processed A-scans. For complex-valued signal

$$\Gamma(i,z) = P(i,z) + i \cdot Q(i,z) \tag{1}$$

and its amplitude

$$A(i,z) = \sqrt{P^2(i,z) + Q^2(i,z)} \tag{2}$$

the mean phase difference between processing A-scans can be found using the Kasai estimator[14]

$$\Delta\varphi = atg\frac{\sum_{z}[P(i,z)Q(i-1,z)-Q(i,z)P(i-1,z)]}{\sum_{z}[P(i,z)P(i-1,z)+Q(i,z)Q(i-1,z)]}, \quad (3)$$

where the *i* and *i-1* are the processed individual A-scans indexes and *z* is the depth. This function is applied subsequently and cumulatively through each row of processing A-scans independently to perform the phase equalization for the all A-scans in each processed sequence. Note, that Kasai estimator is weighted function that takes into account the above-mentioned normalized amplitudes of the pixels. In addition, it requires that all saturated points located primarily on the tissue surface must be subtracted from these pre-processed values to avoid their error-prone unbalanced contributions to phase estimation.

This phase equalization eliminates the mean phase difference between the A-scans that is generally related to the bulk translational motion of the "solid" tissue and retains local phase fluctuations at the vessels caused by Brownian motion or flow. In this way, the phase fluctuations of the block tissue motions are compensated and does not mask the phase fluctuations at the vessels that are caused by local movements of flows of the scatterers.

Figure 2 shows an example of application of this phase equalization approach to compensate phase variations caused by tissue translational motions. Figure 2(a) represents en-face MIP of OCT angiogram of a hamster cheek that was obtained and processed without preliminary phase compensation and Figure 2(b) shows one of B_y-scans (along the processing Y-direction - slow scanning direction) from this angiogram (the B_y-scan cross-section labeled with a white dashed line). Figure 2(c) and Figure 2(d) are plotted for the same dataset but before processing it was passed through the above-described phase-equalization procedure. Figure 2(c) is the *en face* maximum-intensity projection of OCT angiogram and Figure 2(d) is the same B_y-scan as in Figure 2(b). In the latter case (with phase compensation approach), the accuracy of microvasculature detection dramatically increases for the poorly stabilized tissue (which occurs quite often in *in-vivo* measurements). For both cases on Figure 2(a,b,c,d), the procedure of signal normalization is also applied as it was described in the previous section.

In case when the imaged tissue is stabilized by the contacting OCT probe glass window, translational motions become significantly suppressed similarly to the case of fixed window chamber in experiments on animals[15,16]. However, the above-described compensation still improves the images. Here we demonstrate this statement on preliminary results of on-going clinical research on patients treated with radiotherapy. Figure 3 represents *en face* OCT angiograms obtained in 52 seconds from 3x3 mm^2 area of patient's mouth cheek in a probe-tissue contact manner. Figure 3(a) shows the en-face MIP of the 3D data set processed without the preliminary phase compensation, and Figure 3(b) with the phase compensation of the same volumetric dataset. In both cases, all other pre- and post-processing procedures were similarly applied. As a result, the overall SNR of the microcirculation image was improved; bulk tissue motion artifacts represented by spurious horizontal lines in Figure 3(a) were significantly reduced in Figure 3(b).

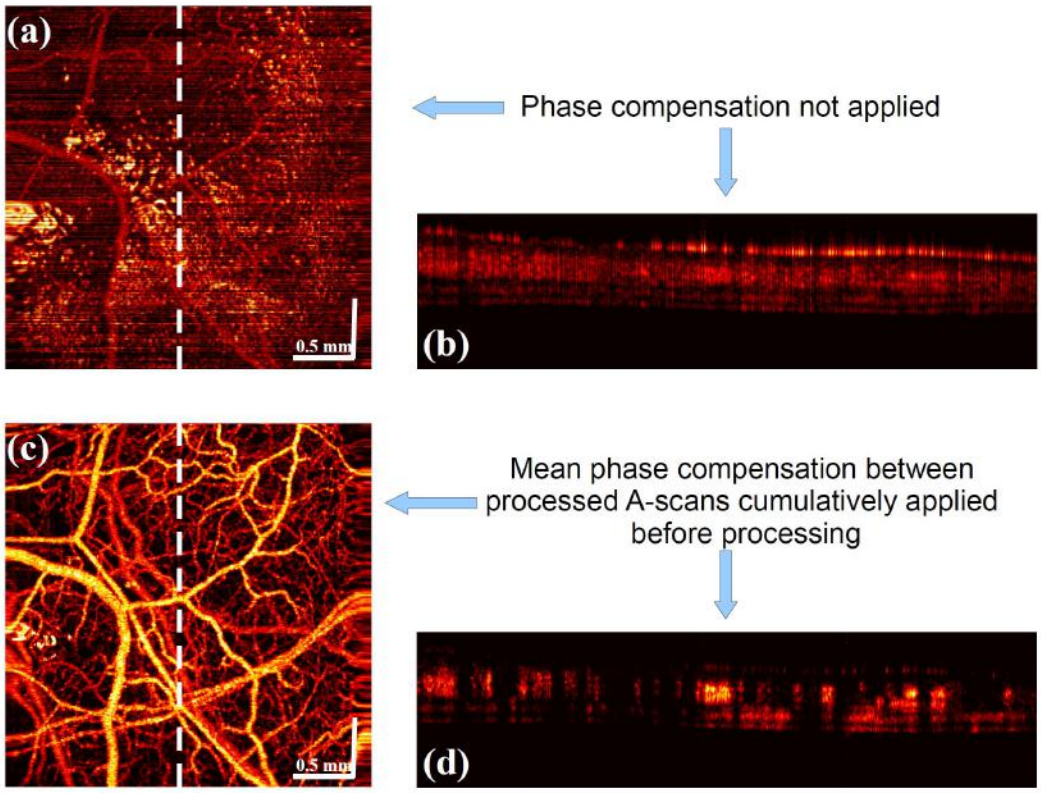

Fig. 2. Examples of efficiency of phase equalization procedure applied to dataset acquired from hamster cheek that was affected by the animal breathing, heart-beating and other translational motions. Panel (a) is the *en face* MIP of OCT angiogram of the hamster cheek acquired and processed without preliminary phase compensation; panel (b) is one of the B_y-scan (along the processing Y-direction) corresponding angiogram (a) and labeled there with a white dashed line. Panel (c) is *en-face* MIP and panel (d) is B_y-scan of the same volumetric dataset but pre-processed with the phase compensation algorithm.

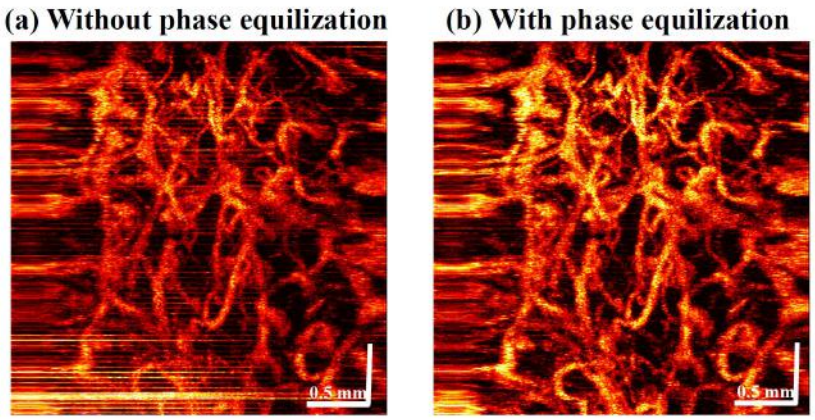

Fig. 3. Example of efficiency of application of phase-equalization approach to data acquired in 52 seconds from 3x3 mm^2 area of radiotherapy treated patient's mouth cheek in a probe-tissue contact manner. Panel (a) demonstrates *en-face* MIP of the 3D data set processed without preliminary phase compensation between A-scans. Panel (b) *en-face* MIP of the same volumetric dataset but pre-processed with the phase compensation algorithm.

4. BINARY MASK AND MAXIMUM VS MEAN (INTEGRAL) INTENSITY PROJECTION

In addition to above-discussed pre-processing techniques, here we consider two post-processing algorithms that also increase SNR and overall quality of microcirculation images. These two possibilities that can be applied additionally to the post-processed dataset are: 1) binary mask based on the Heaviside function to exclude low intensity noisy pixels from the resulting dataset and 2) choosing an appropriate projection type to obtain *en face* microcirculation images. Both operations can be effective but their pros and cons are subject for discussion and depend on particular situation. Namely, average intensity projection provides better isolation of small vessels in very noisy and suffering from artifacts datasets. Such a case is demonstrated in Figure 4 where the angiographic image for insufficiently stabilized hamster cheek is significantly affected by both motion artifacts and glare pixels. Figure 4(a) shows an *en-face* maximum intensity projection (MIP) in which the small vessels are not distinguishable, whereas in Figure 4(b) these vessels become better visible in the average (mean) intensity projection.

In the case of good enough stabilized tissue when only phase compensation is good enough to efficiently eliminate bulk-tissue motion artifacts, the difference between the projection types (maximum intensity projection vs mean intensity projection) is not so significant. The binary mask application in this case only slightly improves the quality of of microcirculation images processed with high-pass filtering of properly normalized complex-valued signals. Figure 5 demonstrates this by four cases applied to the same processed dataset. Figure 5(a) and Figure 5(b) show the maximum intensity projection and mean intensity projection correspondingly without binary mask. Figure 5(c) and Figure 5(d) – the maximum intensity projection and mean intensity projection but both with binary mask.

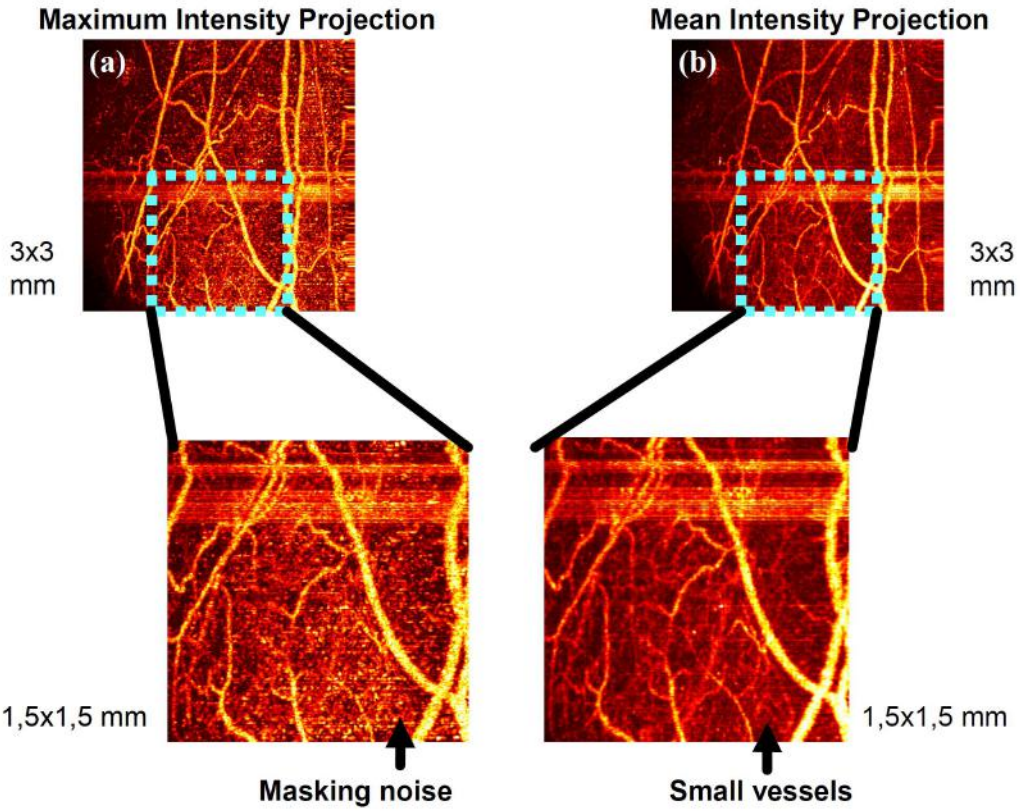

Fig. 4. Comparison of maximum intensity projection and mean (depth-averaged) intensity projection for microcirculation imaging of insufficiently stabilized hamster cheek. Here, phase compensation approach does not reduce everywhere the effect of bulk tissue motion and resulting microvascular image suffers from both motion artifacts and glaring points. Panel (a) demonstrates maximum intensity projection where small vessels are not well distinguishable because of significant masking role of localized artifacts. Panel (b) demonstrates that such vessels become distinguishable in the mean intensity projection. Selected areas with small vessels labeled with blue rectangles in (a) and (b) are enlarged for better visualization.

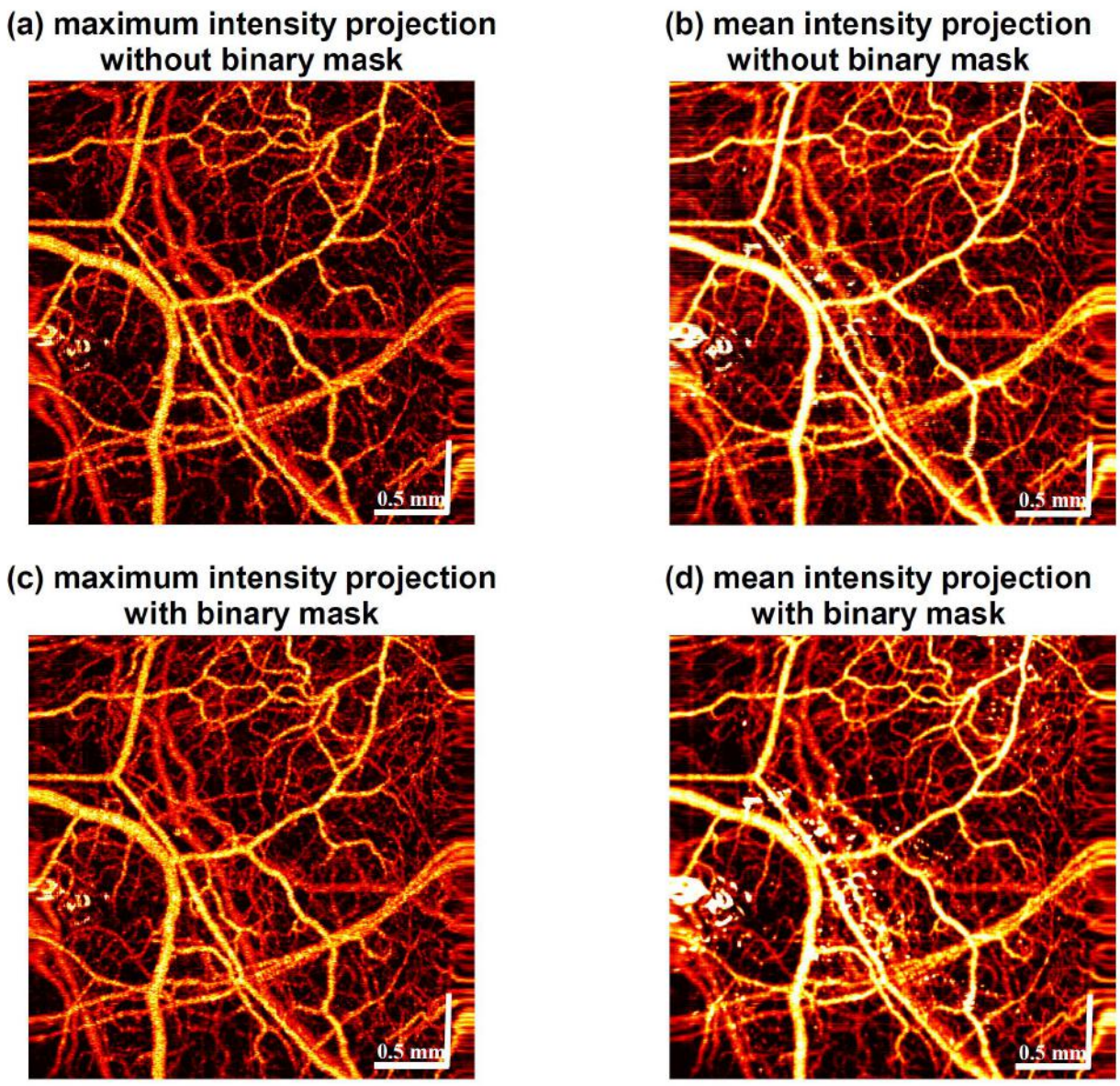

Fig. 5. Difference between application of binary mask and maximum intensity projection versus mean intensity projection. Panel (a) is the maximum intensity projection without binary mask. Panel (b) is the mean intensity projection without binary mask. Panel (c) is the maximum intensity projection with binary mask. Panel (d) is the mean intensity projection with binary mask. Normalization on square root of amplitude and above-mentioned phase equalization using the Kasai estimator were applied before high-pass filtering processing.

5. DISCUSSION AND CONCLUSION

This technical framework complements our recent publications on M-Mode-like OCT algorithms and its implementation[4,5,6,13]. Here we demonstrate importance of pre- and post-processing procedures that can significantly improve the quality of resultant microcirculation images. These procedures in particular involve features of complex-valued signals that naturally combine phase and amplitude information. The proposed normalization of each pixel to its square root temporally-averaged amplitude improves extraction of information contained in phase and amplitude variations for processed data and provides better discrimination of abnormal (e.g., saturated) pixels[5]. The proposed A-scans phase equalization utilizes the following feature of complex-valued A-scans: the phase difference wrapping is not critical, so that phase factors can be equalized very precisely in case of translational displacements that does not exceed resolution of OCT system. It should be additionally emphasized that in the case of more complex motion artifacts described here Kasai phase estimation approach can become a powerful tool to compensate not only subpixel translational displacements but also perform local strain compensations[17]. Also application of binary masks and choosing appropriate type of *en face* plotting can contribute to improve the quality and SNR of the resulting microvasculature images. Combination of these procedures improves significantly vessel-contrast and vessels isolation in the resulting angiograms.

6. ACKNOWLEDGEMENTS

The authors acknowledge support of Russian Foundation of Basic Research (RFBR) grant No 15-42-02513, the Russian Federation Government contract No 14.B25.31.0015 for Leading Scientists and partial support of RFBR grant No 15-29-04851-ofi-m.

REFERENCES

[1] Zaitsev, V. Y., Vitkin, I. A., Matveev, L. A., Gelikonov, V. M., Matveyev, A. L., and Gelikonov, G. V., "Recent Trends in Multimodal Optical Coherence Tomography. II. The Correlation-Stability Approach in OCT Elastography and Methods for Visualization of Microcirculation," Radiophys. Quant. Electron. 57, 210 (2014).
[2] Leahy, M. J., “Microcirculation imaging," ISBN: 978-3-527-32894-9. John Wiley & Sons, 411 pages (2012).
[3] Mahmud, M. S., Cadotte, D. W., Vuong, B., Sun, C., Luk, T. W. H., Mariampillai, A., and Yang, V. X. D., "Review of speckle and phase variance optical coherence tomography to visualize microvascular networks," Journal of Biomedical Optics 18, 050901 (2013).
[4] Matveev, L. A., Zaitsev, V. Y., Gelikonov, G. V., Matveyev, A. L., Moiseev, A. A., Ksenofontov, S. Y., Gelikonov, V. M., Sirotkina, M. A., Gladkova, N. D., Demidov, V., and Vitkin, A., "Hybrid M-mode-like OCT imaging of three-dimensional microvasculature in vivo using reference-free processing of complex valued B-scans," Optics Letters 40(7), 1472 (2015).
[5] Matveev, L. A., Gelikonov, G. V., Matveyev, A. L., Moiseev, A. A., Ksenofontov, S., Gelikonov, V. M., Sirotkina, M. A., Buyanova, N. L., Gladkova, N. D., Demidov, V., Vitkin, A., and Zaitsev, V. Y., "An approach to OCT-based microvascular imaging using reference-free processing of complex valued B-scans," SPIE Proc. 9541, 954106 (2015).
[6] Matveev, L. A., Zaitsev, V. Y., Gelikonov, G. V., Matveyev, A. L., Moiseev, A. A., Ksenofontov, S. Y., Gelikonov, V. M., Demidov, V., and Vitkin, A., "Scan-pattern and signal processing for microvasculature visualization with complex SD-OCT: tissue-motion artifacts robustness and decorrelation time-blood vessel characteristics," SPIE Proceedings 9448, 94481M (2015).
[7] Zaitsev, V. Yu., Matveev, L. A., Gelikonov, G. V., Matveyev, A. L., and Gelikonov, V. M., “A correlation-stability approach to elasticity mapping in optical coherence tomography,” Laser Physics Letters 10(6), 065601 (2013).
[8] Zaitsev, V. Yu., Matveev, L. A., Matveyev, A. L., Gelikonov, G. V., and Gelikonov, V. M., "Elastographic mapping in optical coherence tomography using an unconventional approach based on correlation stability," Journal of Biomedical Optics 19(2), 021107 (2014).
[9] Zaitsev, V. Y., Gelikonov, V. M., Matveev, L. A., Gelikonov, G. V., Matveyev, A. L., Shilyagin, P. A., and Vitkin, I. A., "Recent trends in multimodal optical coherence tomography . I . Polarization-sensitive oct and conventional approaches to OCT elastography," Radiophys. Quant. Electron. 57, 52 (2014).
[10] Matveev, L. A., Zaitsev, V. Yu., Matveyev, A. L., Gelikonov, G. V., and Gelikonov, V. M., “Correlation-stability approach in optical microelastography of tissues,” Proceedings of SPIE 8699, 869904 (2013).

[11] Matveev, L. A., Zaitsev, V. Y., Matveev, A. L., Gelikonov, G. V., Gelikonov, V. M., and Vitkin, A., “Novel methods for elasticity characterization using optical coherence tomography: Brief review and future prospects,” Photonics & Lasers in Medicine 3(4), 295 (2014).
[12] Zaitsev, V. Y., Matveyev, A. L., Matveev, L. A., Gelikonov, G. V., Gelikonov, V. M., and Vitkin, A., "Deformation-induced speckle-pattern evolution and feasibility of correlational speckle tracking in optical coherence elastography," J. Biomed. Opt. 20(7), 075006 (2015)
[13] Gladkova, N. D., Sirotkina, M. A., Buyanova, N. L., Kalganova, T. I., Karabut, M. M., Elagin, V. V., Kuznetsov, S. S., Snopova, L. B., Gelikonov, G. V., Zaitsev, V. Yu., Matveev, L. A., Zagaynova, E. V., and Vitkin, A., "Development of the Methodology of Monitoring Experimental Tumors Using Multimodal Optical Coherence Tomography: the Choice of an Optimal Tumor Model,” Modern Technologies in Medicine 7(2), 6-15 (2015).
[14] Yang, V. X., Gordon, M. L., Mok, A., Zhao, Y., Chen, Z., Cobbold, R. S., Wilson, B. C., and Vitkin, I. A., "Improved phase-resolved optical Doppler tomography using the Kasai velocity estimator and histogram segmentation,” Optics Communications 208(4), 209-214 (2002).
[15] Mariampillai, A., Standish, B. A., Moriyama, E. H., Khurana, M., Munce, N. R., Leung, M. K. K., Jiang, J., Cable, A., Wilson, B. C., Vitkin, I.A., and Yang, Y. X. D., “Speckle variance detection of microvasculature using swept-source optical coherence tomography,” Optics Letters 33, 1530 (2008).
[16] Mariampillai, A., Leung, M. K. K., Jarvi, M., Standish, B. A., Lee, K. K. C., Wilson, B. C., Vitkin, I. A., and Yang, Y. X. D., “Optimized speckle variance OCT imaging of microvasculature,” Optics Letters 35, 1257 (2010).
[17] Zaitsev, V. Y., Matveyev, A. L., Matveev, L. A., Gelikonov, G. V., Gubarkova, E. V., Gladkova, N. D., and Vitkin, A., "Hybrid method of strain estimation in optical coherence elastography using combined sub-wavelength phase measurements and supra-pixel displacement tracking," Journal of Biophotonics, DOI: 10.1002/jbio.201500203 (in print)